Acta Crystallographica Section D
Biological Crystallography
ISSN 0907-4449

Purification, crystallization and X-ray diffraction analysis of a recombinant Fab that recognizes a human blood-group antigen

Shuh-Chyung Song,[a]‡ Kefang Xie,[b]‡ Marcin Czerwinski,[c] Steven L. Spitalnik[a,d] and Joseph E. Wedekind[b]*

[a]Department of Pathology and Laboratory of Medicine, University of Rochester School of Medicine and Dentistry, Rochester, New York 14642, USA, [b]Department of Biochemistry and Biophysics, University of Rochester School of Medicine and Dentistry, Rochester, New York 14642, USA, [c]Ludwik Hirszfeld Institute of Immunology and Experimental Therapy, Wroclaw, Poland, and [d]Department of Pathology, College of Physicians and Surgeons of Columbia University, Room P&S 15-408, 630 West 168th Street, New York, NY 10032, USA

‡ These authors contributed equally to this work.

Correspondence e-mail: joseph_wedekind@urmc.rochester.edu

Received 15 January 2004
Accepted 6 February 2004

The NNA7 Fab fragment recognizes the human glycopeptide N blood-group antigen and has a high affinity for N-type glycophorin A (GPA). To provide insight into how antibodies recognize glycopeptide antigens, soluble Fab fragments were expressed in *Escherichia coli*, purified and crystallized using the hanging-drop vapor-diffusion method at 293 K. The best crystals were obtained from solutions of PEG monomethyl ether 5000 containing 4–8 m*M* yttrium chloride (YCl_3). This rare-earth ion, which could be substituted with various lanthanides, changed the habit of crystals from multi-nucleated rods with a diffraction limit of 4.25 Å resolution to a diamond-shaped morphology that grew as single crystals and diffracted X-rays to 1.75 Å resolution. Data were collected that indicated that the crystals belonged to space group $P2_12_12_1$, with unit-cell parameters $a = 57.9$, $b = 77.1$, $c = 118.1$ Å and one Fab fragment per asymmetric unit. A molecular-replacement solution has been obtained and 86% of the molecule was fitted by use of an automated refinement procedure (*ARP*).

1. Introduction

Glycophorin A (GPA) is the most abundant human red blood cell membrane glycoprotein. GPA is of biomedical relevance because it encodes the M and N blood-group antigens, which are clinically relevant in hemolytic transfusion reactions and hemolytic disease of the newborn (Telischi *et al.*, 1976; Sancho *et al.*, 1998; Parry-Jones *et al.*, 1999). Understanding the antigenicity of the M and N groups (Fig. 1) is complicated by the fact that their epitopes are defined both by amino-acid polymorphisms at positions 1 and 5 of the glycoprotein (Chasis & Mohandas, 1992) and by O-linked glycans at residues 2, 3 and 4 (Lisowska *et al.*, 1980). Although many M- and N-specific monoclonal antibodies have been described (Bigbee *et al.*, 1983, 1984; Jaskiewicz *et al.*, 1990), few studies have examined the humoral immune response to glycopeptide antigens (Hanisch *et al.*, 1995; Karsten *et al.*, 1998). To this end, we focused on studying antibodies that recognize the glycopeptide epitopes comprising the human M and N blood-group antigens (Blackall *et al.*, 1992, 1994). We produced an anti-N Fab fragment, NNA7, the light chain (L) of which was obtained by selection from an Fab phage display combinatorial library, whilst its heavy (H) chain was derived from the parental N92 monoclonal antibody. Consequently, NNA7 retains the immunological characteristics of the N92 hybridoma antibody (Czerwinski *et al.*, 1999) but is amenable to manipulation by molecular-biology techniques (Czerwinski *et al.*, 2002).

The ability to express large amounts of the high-affinity NNA7 Fab fragment makes it an ideal antibody for the study of the interaction between an antibody and its glycopeptide epitope. Such results would have broad implications for biomedical diagnosis and treatment. Here, we report the crystallization and preliminary X-ray diffraction analysis of the NNA7 Fab fragment purified from *Escherichia coli*, as well as progress on its structure determination and refinement. The refined structure of NNA7 along with known mutants that blunt NNA7 reactivity, such as G91S in the L chain of CDR3 (Song *et al.*, 2004), should provide important insights for understanding the molecular basis of antibody specificity for the N-antigen.

2. Materials and methods

2.1. Protein expression and purification

A phagemid encoding the NNA7 Fab fragment was constructed in the pCom3H vector as described previously (Czerwinski *et al.*, 1998). To express a soluble form of the NNA7 Fab fragment, the pComb3H vector containing the cDNA sequences of the NNA7 L-chain and H-chain Fd fragment was restriction-digested with *Nhe*I and *Spe*I (Roche Diagnostics Co., IN, USA), thereby removing the bacteriophage

	1	2	3	4	5
M	NH_3-Ser	Ser	Ser	Thr	Gly
N	NH_3-Leu	Ser	Ser	Thr	Glu

Figure 1
Positions 1–5 of the M and N blood-group antigens.

Table 1
X-ray diffraction intensity statistics for Fab NNA7.

Values in parentheses correspond to reflections in the highest resolution shell.

Resolution range (Å)	1.83–36.7 (1.83–1.90)
Space group	$P2_12_12_1$
Unit-cell parameters (Å, °)	a = 57.9, b = 77.1, c = 118.1, $\alpha = \beta = \gamma$ = 90
No. molecules per AU	1 (450 amino acids)
Unit cell volume (Å^3)	527147
Solvent content (%)	56.4
Total No. reflections	160483
No. unique reflections	43775
Average redundancy	3.7 (1.4)
Completeness (%)	92.4 (53.0)
R_{sym}† (%)	6.5 (29.3)
$I/\sigma(I)$	12.9 (2.4)

† $R_{sym} = [\sum |I(h)_j - \langle I(h)\rangle| / \sum I(h)_j] \times 100$, where $I(h)_j$ is the observed intensity of the jth measurement of reflection h and $\langle I(h)\rangle$ is the mean intensity of reflection h.

gene III fragment, followed by religation using T4 ligase (Roche Diagnostics Co.). In addition, a 6×His affinity tag was added to the 3′ end of the H-chain Fd fragment. The resulting vector was electroporated into *E. coli* SURE cells (Stratagene, CA, USA) that were subsequently plated onto LB–carbenicillin plates. Cells isolated from a single colony were grown at 310 K overnight in 0.01 l Super Broth medium supplemented with 50 µg ml^{-1} carbenicillin and 10 µg ml^{-1} tetracycline (Czerwinski *et al.*, 1998). The next day 500 µl aliquots from these cultures were inoculated into 0.2 l Super Broth containing 50 µg ml^{-1} carbenicillin, 0.1% glucose and 0.020 *M* $MgCl_2$ and incubated at 310 K until the OD at 600 nm reached 0.2. IPTG was added to a final concentration of 1 m*M*, followed by incubation at 295 K for an additional 12–16 h. Cells were harvested by centrifugation at 6000*g* for 15 min and periplasmic proteins were released by use of the B-PER bacterial protein-extraction reagent (Pierce, IL, USA). The lysate was centrifuged at 40 000*g* for 50 min and the supernatant was dialyzed extensively against 0.050 *M* NaH_2PO_4/Na_2HPO_4 with 0.30 *M* NaCl buffered at pH 8.0.

The soluble NNA7 Fab fragments were collected from 0.5 l bacterial cell lysate and purified by the use of Ni–NTA resin (Qiagen, CA) using wash and elution buffers at pH 6.5; the protein was eluted with 0.10 *M* imidazole. The elutant from the Ni–NTA column was dialyzed against 0.050 *M* NaH_2PO_4/Na_2HPO_4 pH 8.0 and loaded onto a 1 ml column of Q-Sepharose (Amersham Pharmacia Biotech, Sweden). The flow-through from the column contained the soluble Fab fragments. This material was adjusted to 0.30 *M* NaCl and then loaded and re-eluted from Ni–NTA agarose (as described previously). The two-step purification was repeated as necessary in order to obtain pure protein. Following dialysis against 0.020 *M* Tris–HCl pH 8.0 containing 0.15 *M* NaCl, the protein was concentrated to 6 mg ml^{-1} using a Micro-ProDiCon ultrafiltration system (Spectrum, TX, USA). The final protein content was measured using the bicinchoninic acid protein assay (Pierce, IL, USA) and the purity of the protein preparation (∼90%) was confirmed by SDS–PAGE under reducing and non-reducing conditions, as described by Czerwinski *et al.* (2002). The average protein yield per preparation is about 300 µg l^{-1}.

2.2. Crystallization

Purified NNA7 Fab fragment was dialyzed against 0.10 *M* sodium cacodylate buffer pH 6.0 with 0.15 *M* ammonium acetate and immediately used for crystallization. The NNA7 Fab fragment was screened for crystallization using the hanging-drop vapor-diffusion method at 277 and 293 K with 2 µl protein solution and an equal volume of screening reagent. Drops were equilibrated against 1 ml mother-liquor reservoir solution contained within the Crystal Tool (Nextal Biotech, QC, Canada). Crystal Screen II and the Sodium/Potassium Phosphate Quick Screen (Hampton Research, CA, USA) were used. The best crystals grew as multinucleated clusters after 6 d at 293 K from solutions consisting of $(NH_4)_2SO_4$, polyethylene glycol monomethyl ether 5000 (PEG MME 5K) and MES buffer. Based on these conditions, screens were conducted by varying the pH, salt and PEG concentrations. To further improve the crystals, Additive Screen 1 (Hampton Research, CA, USA) was employed as described by the manufacturer.

2.3. X-ray diffraction experiments

As a prelude to X-ray diffraction analysis, crystals were cryoprotected by serial transfers into synthetic mother liquor containing 20%(*v*/*v*) PEG MME 5K and either 5, 10, 15 or 20%(*v*/*v*) glycerol. Crystals were mounted in 10 µm diameter rayon loops (Hampton Research) and flash-cooled by exposure to a stream of nitrogen gas at 95 K generated by an X-Stream system (Rigaku/MSC, Japan). X-ray diffraction data were collected from single crystals using Cu $K\alpha$ radiation generated by an RU-H2R rotating-anode generator (Rigaku/MSC, Japan) operated at 4.5 kW. X-rays were monochromated and focused with confocal Blue optics (Osmic, MI, USA) and passed through a collimator with a 300 µm front-end pinhole. Intensities were recorded on an R-AXIS IV image-plate detector (Rigaku/MSC) with a vertical φ-axis. High-resolution data were recorded at a distance of 165 mm as 90 × 1° oscillations. Because of spatial overlaps, a low-resolution data set was recorded at a distance of 195 mm as 30 × 1° oscillations. All exposure times were 60 min. Intensities were reduced and scaled with the *CrystalClear* v.1.3.5 software package (Pflugrath, 1999). The intensity statistics for the X-ray diffraction data are summarized in Table 1.

2.4. Molecular replacement

A molecular-replacement solution for the NNA7 Fab fragment was obtained using *AMoRe* (Navaza, 1994). The search model was the crystal structure of 48G7 (PDB code 1aj7), an Fab fragment that was expressed in *E. coli* as a chimeric protein comprising the mouse V_H and V_L regions fused to human C_H1 and C_K constant regions, respectively (Wedemayer *et al.*, 1997). A two-fragment search was conducted by dividing the structure of 48G7 into its variable-region residues (1–105 of the L chain combined with 1–111 of the H chain) and constant-region residues (111–214 of the L chain and 116–216 of the H chain). All amino acids of 48G7 were included in the search model except the intervening hinge sequences between the variable and constant regions.

2.5. Automated model building

The molecular-replacement solution was subjected to 7500 K torsional annealing as implemented in *CNS* (Brünger *et al.*, 1998; final R_{factor} = 37.1% and R_{free} = 44% for data in the resolution range 2.65–25 Å). The resulting model was utilized in automated model building using diffraction data in the resolution range 1.9–25 Å as implemented in *ARP/wARP* v.6 (Perrakis *et al.*, 1999). The initial mode was 'automated building starting from a model'. Refinement took place using *REFMAC*5 (Collaborative Computational Project, Number 4, 1994) in 'slow' mode using an R_{free} test set of 8%. The 'breadth first' C_α-recognition option was selected. Docking of the autotraced chain to the amino-acid sequence was implemented after six cycles of autobuilding.

3. Results and discussion

3.1. Crystallization

In order to conserve the amount of NNA7 Fab fragment consumed in crystallization trials, initial screens were compiled from

previously reported Fab structures deposited in the Protein Data Bank (Berman *et al.*, 2000). The compiled conditions included various salts such as $(NH_4)_2SO_4$ or NaCl combined with PEG 6000 and divalent ions such as $CoCl_2$. Combinations of these precipitants were employed in screens over the pH range 6.5–8.0, but this approach yielded no suitable crystals. Therefore, a broader set of conditions was examined by use of the incomplete factorial compilation in Crystal Screen 2 (Hampton Research). Crystals appeared after 10 d at 293 K in solutions consisting of 0.10 *M* MES pH 6.5, 0.20 *M* ammonium sulfate and 30%(*v*/*v*) PEG MME 5K. Subsequently, different concentrations of ammonium and sulfate salts including $(NH_4)_2SO_4$, ammonium acetate, NH_4Cl and Li_2SO_4 were screened in the presence of various PEG polymers. These efforts led to conditions consisting of 22–24%(*w*/*v*) PEG MME 5K in 0.10 *M* MES buffer pH 6.5 with 0.30 *M* $(NH_4)_2SO_4$ that gave rise to rod-shaped crystal clusters (Fig. 2*a*). A few single crystals were obtained, but these only diffracted X-rays anisotropically to 4.25 Å resolution. To further improve the quality of the crystals, Additive Screen 1 (Hampton Research) was employed, resulting in tetragonal bipyramidal crystals that grew from solutions of YCl_3 after three weeks. Based on this condition, we optimized the YCl_3 concentration and evaluated the effect of other rare-earth metals including $LuCl_3$, $SmCl_3$ and $NdCl_3$ from the lanthanide series. The best crystals grew in a tetragonal bipyramidal habit from solutions of 2–8 m*M* Y^{3+} or Sm^{3+} (Fig. 2*b*).

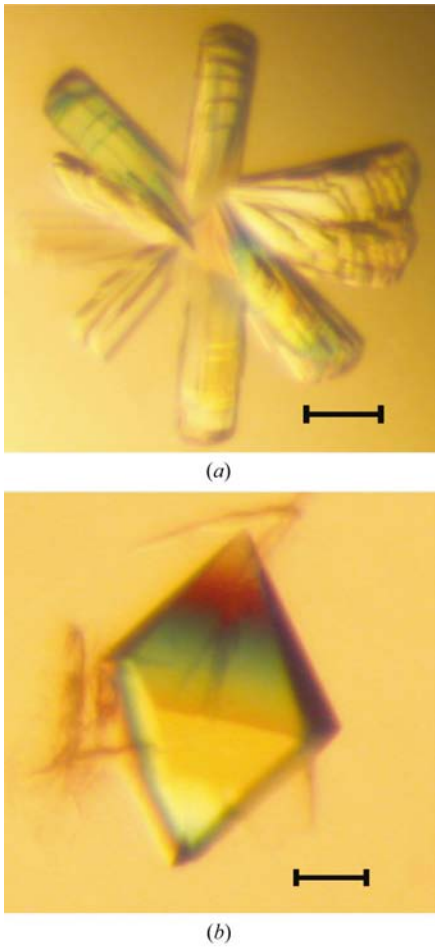

Figure 2
Representative digital images of NNA7 Fab crystals photographed under polarized light. (*a*) Rod clusters; the black bar is 25 µm. (*b*). Bipyramidal-shaped crystals grown under the same conditions as (*a*) except with 8 m*M* YCl_3 as an additive. The black bar is 50 µm.

3.2. X-ray data reduction

The best crystals of the NNA7 Fab fragment diffracted X-rays to 1.75 Å resolution on our in-house source. Complete X-ray diffraction data were recorded to 2.0 Å resolution, which represents the edge of the image plate at 165 mm (Fig. 3). Additional data were recorded in the plate corners to a level of 53% completeness in the 1.83–1.90 Å resolution shell (Table 1). The high $I/\sigma(I)$ value of 2.4 in the highest resolution shell indicated that higher resolution data could have been obtained, which should be relevant to future studies of the antibody–antigen complex. The space group of NNA7 Fab was assigned based upon the autoindexing method employed in *CrystalClear*, which suggested a primitive orthorhombic Bravais lattice with unit-cell parameters $a = 57.9, b = 77.1, c = 118.1$ Å, $\alpha = \beta = \gamma = 90^\circ$. This assignment was consistent with the 2/*m* by 2/*m* reciprocal-lattice symmetry along the principal axes of the major zones *hk*0, *h*0*l* and 0*kl* (Fig. 3). The presence of systematic absences of the form $2n + 1$ from the *h*00, 0*k*0 and 00*l* reflection classes suggested the presence of 2_1 screw axes indicative of space group $P2_12_12_1$. The resulting V_M (Matthews, 1968) was 2.8 $Å^3\ Da^{-1}$ (solvent content 56.4%), corresponding to one 46.7 kDa NNA7 Fab fragment per asymmetric unit.

3.3. Molecular replacement

The structure of NNA7 was solved by molecular replacement by the use of a well refined Fab fragment, 48G7, as a search model. The 48G7 and NNA7 Fab fragments have an overall sequence identity of 47% (62.4% homology). In order to solve the structure of NNA7, it was necessary to divide the search model into its variable and constant regions. The variable regions of the L and H chains exhibited 55 and 39.6% sequence identity (68.6 and 61.3% homology) to those of the NNA7 Fab, whereas the constant regions of the L and H chains were 60.2 and 70% identical (87.4 and 84% homologous) to NNA7. The search was conducted using X-ray data between 3.0 and 15 Å resolution and resulted in a top solution with a correlation coefficient of 45.5 and an *R* factor of 47.8%. The solution had Euler angles $\alpha = 127.3, \beta = 162.1, \gamma = 149.9^\circ$ with a translational component $X = 27.3, Y = 18.8, Z = -13.3$ Å for the constant region and $\alpha = 77.4, \beta = 130.3, \gamma = 280.0^\circ$ with $X = 0.1, Y = 48.9, Z = 51.6$ Å for the variable region after rigid-body refinement. The next highest solution was false, with a correlation coefficient of 36.7 and an *R* factor of 51.1%. A comparison of C_α residues from the resulting NNA7 structural solution with the coordinates of the search model revealed a significant conformational change in the relative positions of the constant and variable domains. This change corresponded to a rigid-body hinge motion of 12° between the domains and accounted for the fact that the NNA7 structure could not be solved without dividing the search model into its respective variable and constant regions.

3.4. Automated model building

The software package *ARP*/*wARP* was used to fit the NNA7 L- and H-chain sequences into electron-density maps phased by molecular replacement. Nearly 86% of the molecule was fitted and among these regions 74% were correct sequences, 2% were fitted with either poly-Gly or poly-Ala and the rest were modeled as dummy atoms (Fig. 4). Overall, the software had a high success rate in building, but minor

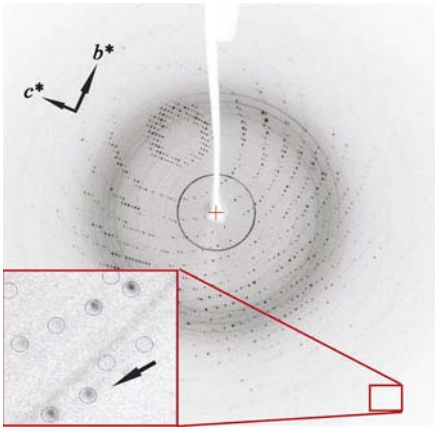

Figure 3
Representative X-ray diffraction image of an NNA7 Fab crystal. The inset box is enlarged. Maximum resolution in the corner of the plate is 1.75 Å. Observed reflections are overlaid with the predicted diffraction pattern (blue circles). An arrow indicates Bragg diffraction at 1.88 Å resolution.

mistakes were present. In one instance, two β-strands were built into a crystallographically related molecule. Additionally, a poly-Gly region of the first β-strand was traced with incorrect strand directionality. Interestingly, this portion of the structure was present in the initial search model, but was removed and later added back by *ARP*/*wARP*. This error was most likely to have arisen from a combination of two factors. Firstly, the location of the strand at the immediate N-terminus of the protein may have resulted in a lack of restraints for a proper main-chain connectivity assignment. More importantly, although the electron density of this region appeared to be ordered, the β-strand was of poorer quality in terms of its signal-to-noise (electrons per Å^3) compared with the core structure. This attribute may have resulted in a poor probability score for the initial model that led to its removal and subsequent replacement with poly-Gly. Errors in these regions were detected by comparison of the *ARP*/*wARP* model to the known immunoglobulin fold and the observation that strand termini were positioned head-to-head rather than head-to-tail for peptide-bond formation. Manual structural refinement is under way. The final R factor and $R_{\rm free}$ values resulting from *ARP*/*wARP* were 20.6 and 30.4%, respectively. A portion of the electron-density map and the hybrid from automated building is shown in Fig. 4.

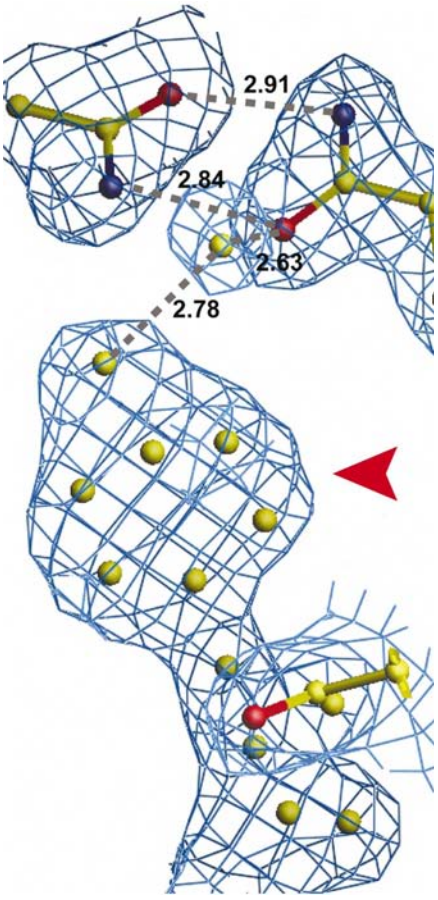

Figure 4
Representative portion of a ($2F_o - F_c$) electron-density map contoured at the 1.2σ level using $\alpha_{\rm calc}$ from a hybrid model produced by *ARP*/*wARP*. The resolution range for the calculation was 25–1.9 Å. A portion of the model is shown with a tyrosine residue (red arrowhead) modeled with 'dummy' atoms (isolated yellow spheres). Amino acids for two glutamines are indicated by ball-and-stick models (bonded blue, red and yellow spheres are N, O and C atoms, respectively). Dashed lines with labeled distances indicate potential hydrogen bonds. A solvent molecule bridges the tyrosine hydroxyl group and the O atom of the glutamine amide moiety. This figure was prepared using *O* (Jones *et al.*, 1991).

It is interesting to speculate that the use of YCl_3 may have a general role in improving the diffraction properties of Fab crystals. Thus far, only one other Fab structure has been described in the presence of Y^{3+}. However, unlike our study, in which YCl_3 was employed as a crystallization additive, the existing Fab structure indicated Y^{3+} to be part of the antigenic complex bound in the variable region (Corneillie *et al.*, 2003). Therefore, until our NNA7 structure is refined, the location and role of rare-earth ions in Fab crystallization remain unknown.

In conclusion, the additive YCl_3 increased X-ray diffraction of NNA7 Fab crystals from 4.25 to 1.75 Å resolution. A high-resolution data set was collected to 1.83 Å and the Fab fragment structure was solved by molecular replacement. The high quality of the data allowed automated model building by use of *ARP*/*wARP*, which fitted 86% of the protein atoms. An examination of minor errors in the NNA7 hybrid model suggested that studies utilizing automated building methods should carefully scrutinize the veracity of N- and C-terminal structures comprising β-strands. Overall, this work represents preliminary progress in our efforts to understand the molecular determinants leading to antibody recognition of the human N glycopeptide blood-group antigen. High-resolution structural information should prove useful in combination with molecular-biology techniques in the rational design of antibodies with high affinity and high specificity for targets that require serological testing in transfusion medicine.

The authors thank one of the reviewers for interest and insight regarding the results of *ARP*. This work was supported by NIH grants P01 HL54516 (SLS) and RR 15934 (JEW), by a grant (6 P04A 05621) from the Committee for Scientific Research (KBN), Warsaw, Poland (MC) and by institutional support from the University of Rochester (JEW and SLS).

References

Berman, H. M., Westbrook, J., Feng, Z., Gilliland, G., Bhat, T. N., Weissig, H., Shindyalov, I. N. & Bourne, P. E. (2000). *Nucleic Acids Res.* **28**, 235–242.
Bigbee, W. L., Langlois, R. G., Vanderlaan, M. & Jensen, R. H. (1984). *J. Immunol.* **133**, 3149–3155.
Bigbee, W. L., Vanderlaan, M., Fong, S. S. & Jensen, R. H. (1983). *Mol. Immunol.* **20**, 1353–1362.
Blackall, D. P., Ugorski, M., Smith, M. E., Pahlsson, P. & Spitalnik, S. L. (1992). *Transfusion*, **32**, 629–632.
Blackall, P. J., Ugorski, M., Påhlsson, P., Shakin-Eshelman, S. H. & Spitalnik, S. L. (1994). *J. immunol.* **152**, 2241–2247.
Brünger, A. T., Adams, P. D., Clore, G. M., DeLano, W. L., Gros, P., Grosse-Kunstleve, R. W., Jiang, J.-S., Kuszewski, J., Nilges, M., Pannu, N. S., Read, R. J., Rice, L. M., Simonson, T. & Warren, G. L. (1998). *Acta Cryst.* D**54**, 905–921.
Chasis, J. A. & Mohandas, N. (1992). *Blood*, **80**, 1869–1879.
Collaborative Computational Project, Number 4 (1994). *Acta Cryst.* D**50**, 760–763.
Corneillie, T. M., Fisher, A. J. & Meares, C. F. (2003). *J. Am. Chem. Soc.* **125**, 15039–15048.
Czerwinski, M., Krop-Watorek, A., Lisowska, E. & Spitalnik, S. L. (2002). *Transfusion*, **42**, 257–264.
Czerwinski, M., Krop-Watorek, A., Siegel, D. L. & Spitalnik, S. L. (1999). *Transfusion*, **39**, 364–371.
Czerwinski, M., Siemaszko, D., Siegel, D. L. & Spitalnik, S. L. (1998). *J. Immunol.* **160**, 4406–4417.
Hanisch, F. G., Stadie, T. & Bosslet, K. (1995). *Cancer Res.* **55**, 4036–4040.
Jaskiewicz, E., Moulds, J. J., Kraemer, K., Goldstein, A. S. & Lisowska, E. (1990). *Transfusion*, **30**, 230–235.
Jones, T. A., Zou, J. Y., Cowan, S. W. & Kjeldgaard, M. (1991). *Acta Cryst.* A**47**, 110–119.
Karsten, U., Diotel, C., Klich, G., Paulsen, H., Goletz, S., Muller, S. & Hanisch, F. G. (1998). *Cancer Res.* **58**, 2541–2549.
Lisowska, E., Duk, M. & Dahr, W. (1980). *Carbohydr. Res.* **79**, 103–113.
Matthews, B. W. (1968). *J. Mol. Biol.* **33**, 491–497.
Navaza, J. (1994). *Acta Cryst.* A**50**, 157–163.
Parry-Jones, N., Gore, M. E., Taylor, J. & Treleaven, J. G. (1999). *Clin. Lab. Haematol.* **21**, 407–408.
Perrakis, A., Morris, R. & Lamzin, V. S. (1999). *Nature Struct. Biol.* **6**, 458–463.
Pflugrath, J. W. (1999). *Acta Cryst.* D**55**, 1718–1725.
Sancho, J. M., Pujol, M., Fernandez, F., Soler, M., Manzano, P. & Feliu, E. (1998). *Br. J. Haematol.* **103**, 268–269.
Song, S. C., Czerwinski, M. & Spitalnik, S. L. (2004). *Transfusion*, **44**, 173–186.
Telischi, M., Behzad, O., Issitt, P. D. & Pavone, B. G. (1976). *Vox Sang.* **31**, 109–116.
Wedemayer, G. J., Patten, P. A., Wang, L. H., Schultz, P. G. & Stevens, R. C. (1997). *Science*, **276**, 1665–1669.